Ultrasound Image-to-Patient Registration in Neurosurgery

Mariana Milhano Pinto Elyseu
mariana.elyseu@tecnico.ulisboa.pt

Instituto Superior Técnico, Lisboa, Portugal

June 2018

Abstract

Neuronavigation Systems have caused a profound impact on neurosurgical practice and revolutionised its workflow over the past decades. These systems allow surgeons to identify the structure they are working on by navigating real time through a virtual 3D reconstruction of the patient's brain, based on preoperative images. Image-to-patient registration is a crucial step in navigation systems. It is the accurate alignment of the preoperatively acquired imaging data to the patients neuroanatomy inside the operating room, creating a linkage between virtual and morphological data. It generates a common coordinate system that allows any point in the image coordinate system to be transferred into the surgical coordinate system and vice versa. However, current registration methods present a few drawbacks. The present work suggests a new registration technique that uses the Iterative Closest Point algorithm to register preoperative CT images with intraoperative US ones. This is a non-invasive method, easily incorporated in a surgical environment, that surpasses obstacles presented by current registration techniques. It is tested in a laboratory environment with a phantom that resembles a mean dimensioned human skull.
Keywords: Neuronavigation, Segmentation, Registration, Ultrasound, Iterative Closest Point.

1. Introduction

Up to the end of the 1980s, Frame-based Stereotactic Systems were the standard method for accurately localising small intracranial lesions [1]. In contrast, since then the use of computer-assisted systems in Neurosurgery has started to evolve as an attempt to follow the movement of surgical instruments in real time on the "image space" recreated in computer. Neuronavigation Systems (or Frameless Stereotactic Systems) have caused a profound impact on neurosurgical practice and revolutionised its workflow over the past decades, by replacing stereotactic frames by surgical tracked instruments and showing benefits in improved planning and performance of Image-Guided Neurosurgery [2, 3, 4, 5, 6].

Every neuronavigation procedure follows similar stages. The first one is preoperative imaging capture, for instance using Computed Tomography (CT) and/or Magnetic Resonance Imaging (MRI). Then, a virtual 3D reconstruction of the patients head is created by the neuronavigation system software, allowing the surgeon to visualise and "navigate" inside the patient's brain. This way, the surgeon can plan the intervention, choosing an entry point and the best trajectory the surgical instrument may follow to reach the desired target location, either to be biopsied or to place a deep brain electrode [6, 7, 8]. Meanwhile, the patient is lied down inside the surgical theatre. At this point, the relation between the virtual imaging data and the real patients body is still unknown. So the following step, performed inside the operating room and before the surgical intervention, aims to find a correlation between them so that any point in the surgical space can be associated with its corresponding coordinates in the image space. This procedure is called Image-to-Patient Registration and represents the second step of the neuronavigation procedure.

Once the registration is successfully done, any surgical instrument recognised by the tracking device can be tracked in the surgical space and visualised real-time in the image space. This way, during the entire procedure the surgeon can see the instruments tip on the monitor of the computer workstation in the axial, sagittal and coronal plans, as well as in the volume reconstruction over all.

2. State-of-the-Art: Registration Techniques for Computer Navigation

Image-to-patient registration is a crucial step in navigation systems [9, 7, 10, 11]. It should be performed cautiously since it has a direct effect onto performance, accuracy and precision of all following navigational tasks [12, 5, 9, 3, 7].

Registration is the accurate alignment of the preoperatively acquired imaging data - known as image

space - to the patients neuroanatomy inside the operating room - surgical space -, creating a linkage between virtual and morphological data. This way, any point in one coordinate system can be transferred into the other coordinate system and vice versa. That is to say, it generates a common coordinate system.

In neuronavigation systems a wide range of image-to-patient registration techniques have been developed. Suggested by some literature [5, 3, 13], one way to group them can be: point-based and surface-based registration methods, described below.

2.1. Point-based Registration

Point-based registration methods require landmarks, also called fiducials. Figure 1 shows the sequence of the fiducials' recognition in the image space, its identification with a pointer recognised by a tracking device in the surgical space, where the patient is lied down, and the result of the registration, expressed in the image space coordinate system. This correspondence is assumed to be known thanks to the presence of the same features in both spaces. Also, the number of fiducials together with their spatial distribution are the key to the registration accuracy optimisation [13, 3, 10, 14, 15].

Figure 1: Point-based Registration [16].

2.1.1 Natural Fiducials

Using external natural anatomical landmarks, also called natural fiducials - such as the tip nose or the internal and external limits of the eye -, to register images to patients is the most simple and easy way [5, 11]. Here, a pointer that is recognised by the tracking device is used to identify the landmarks in the surgical space. Then, the neuronavigation software associates both landmarks as being the same by the calculation of a transformation matrix.

2.1.2 Synthetic Fiducials

It is also possible to use external synthetic fiducials for registration, either with self-adhesive markers glued to the skin or markers rigidly screwed to the patients scalp under local anaesthesia.

Generally speaking, synthetic fiducials are applied to the patients head before image acquisition and, since they are clearly identifiable in CT and MRI, they can be recognised within the image data set as long as they were made visible during image acquisition. Then, without being moved or removed from the patients head, they are digitised in the operating room again with a trackable pointer so that each fiducial is identified in both image and surgical spaces to be registered. After that, the neuronavigation software determines the transformation matrix from one coordinate system to another.

2.2. Surface-based Registration

On the other hand, surface-based registration methods use two large number point sets - from hundreds to thousands points - describing the same surface. As shown in Figure 2, in this type of registration skin surface is obtained through image segmentation in the image space (for example with contouring algorithms), a large number of points is collected manually in the surgical space and, then, a transformation matrix is determined in order to fit the acquired point cloud onto the skin surface. Unlike point-based methods, the correspondence of points between image and surgical spaces is not known and, in view of being optimal, some measure of distance should be minimal while some similarity function should be at its maximum [5].

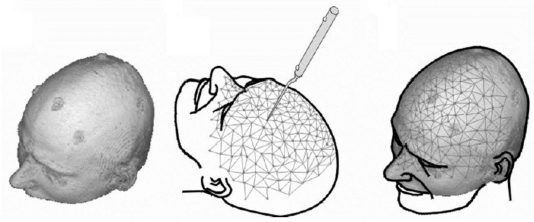

Figure 2: Surface-based Registration [16].

2.2.1 Recognition of the face contour

One of the surface-based registration methods is the recognition of the face contour by manually touching the skin surface with a tracking pointer recognised by the navigation system. This pointer goes around the nose, forehead, ears and other structures [11], and its trajectory sometimes is random and chosen by the surgeon, sometimes has to mimic some path indicated by the navigation system.

2.2.2 Laser Scanning

Another registration method based on surface matching relies on the use of a laser. Some methods use a laser beam to project lines and/or textured patterns onto the patients face, that are then read by a system equipped with a camera [17, 5]. Others use a laser pointer that is tracked by a navigation system. The dot projected on the patients face, as it moves around randomly, is recognised by

the tracking system, allowing to measure distances and positions and the construction of a 3D model. Laser surface scanners are more accurate than laser pointers because they acquire a larger number of points [5].

2.3. Quantifying Registration Accuracy

In order to evaluate and compare the several registration techniques' accuracy, Fitzpatrick et al.[18] suggested both Registration Error (RE) and Target Registration Error (TRE) for a systematic analysis of registration errors.

RE denotes the distance between the "real" surface position in the surgical space and its counterpart in the image space after being registered. RE provides a measure of registration quality. At the same time, TRE refers to the distance between the real target position and its final position after registration. So, TRE provides the "real" error of the surgical procedure. The used distance metrics is the Euclidean distance.

However, it is not possible to compare the presented registration techniques' accuracy using RE or TRE because these values vary not only according to the considered fiducial number and their spatial distribution, but also differ among hospitals and even in the same hospital with the same technique but different clinical cases [19, 20, 17]. Even though, these metrics can and will be used throughout this work to compare results among them.

3. Proposed project

Current image-to-patient registration methods present a few drawbacks. By one side, point-based registration techniques are all very limited by the small number of points considered for registration and some authors [3] refer to fiducial registration methods as being time consuming since the surgeon has to manually identify the points. Besides, natural fiducials are very susceptible to errors - for instance, in the preoperative selection of points and the precise identification of their counterparts -, skin synthetic and natural fiducials are not fully reliable as the skin can shift and suffer deformation and bone synthetic fiducials are invasive and require new preoperative images exposing the patient to an extra dose of radiation when CT is used. By the other side, surface-based registration techniques, like face contour and laser scanning, are also strongly influenced by skin shift and deformation.

Given these points, the present work suggests a new registration technique that surpasses obstacles presented by current registration techniques, using preoperative CT images with intraoperative ultrasound (US) ones. Since both CT and US can directly identify the outer skull surface, without skin limitations, they can be used as a combined registration technique. Additionally, US scans acquire a large number of points, are non-invasive, require no radiation and are easily incorporated in a surgical environment. In this work, two variants of the Iterative Closest Point algorithm are used and RE and TRE are computed to evaluate the suggested registration technique accuracy.

The remainder of this paper is organised as follows. Section 4 presents the materials and methods used in this work. Section 5 describes the segmentation algorithms' steps used to extract the outer skull surface from both CT and US images. Section 6 gives a detailed overview of two proposed algorithms for registration. Section 7 shows the results and discusses them. Finally, Section 8 summarises the paper, enhancing its main conclusions.

4. Materials and Methods

4.1. Devices

- Passive Polaris Spectra System

The Passive Polaris Spectra System is an optical tracking device, developed by Northern Digital, that detects and records both the position and orientation (pose) of objects in space through time. Any surgical instrument can be tracked by Polaris as long as they has a rigidly fixed tool with markers attached that reflect the infrared light emitted by Polaris' cameras. This way, the system localises the position and orientation of the tools in relation to the Polaris base reference frame and tracks them with high accuracy.

- ProSound 2 US machine

ProSound 2 is an analogical portable ultrasound system developed by Hitachi Aloka. The linear US probe UST-586-5, commercialised by the same group, is used. This probe gives rise to 2D images and shows the analysed structures' anatomy in sectional, or tomographic, images obtained in any spacial orientation.

- Frame Grabber

ProSound 2 does not include an interface to acquire digital images directly. It needs to be connected to a computer via an electronic device called frame grabber. This device grabs individual frames from an analogical video signal and transmits them to the computer. The Video Editor USB Deluxe frame grabber, commercialised by Not Only TV, is used.

- CT Scanner

Philips Brilliance R 64 CT scanner, from Hospital Santa Maria in Lisbon, is used. The CT images are stored in DICOM (Digital Imaging and Communications in Medicine) format.

4.2. Case study

In this thesis a head phantom is used as case study. A phantom is a synthetic model of the body or of a

body specific part. In this case, it is a synthetic human skull model, represented in Figure 3, designed in SolidWorks® and 3D printed. Its overall dimensions resemble an average human head: 305 mm up-down, 178 mm left-right and 203 mm anterior-posterior.

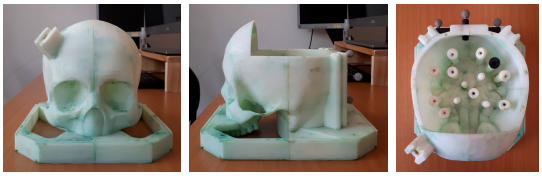

(a) Front view (b) Side view (c) Top view

Figure 3: Human skull phantom.

Inside the phantom cranial cavity there is a set of 14 structures intended to simulate internal tumours, or surgical targets. In this work only the 10 that have a spherical shape with a hollow hole in the centre will be considered, since only these can be characterised not only by their position, but also by their orientation in space.

4.3. Experimental setup

4.3.1 Devices' assembly

- Junction of a Polaris tool with US probe

In order to obtain US images with poses relative to the Polaris base reference frame, the optical tracking tool 8700339 must be coupled to the US probe so that it can be tracked and ${}^{Polaris}_{USprobe}T$ can be recorded.

- Probe-image calibration

Polaris can only track the pose of the tool attached to the US probe, and not the US image planes themselves. This way, a probe-image calibration must be performed. Calibration is the process of computing the transformation (rotation and translation) between the US probe and the US images, ${}^{USProbe}_{USimg}T$, essential to map every pixel in an image in the US probe referential. Here, a calibration technique using a pointer is used [21].

- Junction of a Polaris tool with phantom

The 8700449 optical tracking tool must be also coupled to the phantom so that its poses can be recorded in Polaris reference frame, ${}^{Polaris}_{phantom}T$, and the US images can have its poses in relation to the phantoms reference frame. This way the phantom does not need to me immobilised and its motion can be tracked as well and compensated by the system.

4.3.2 US images' acquisition

From the previous calibrations, one can compute the US images' localisation in the phantom reference frame, ${}^{phantom}_{USimg}T$, so that:

$$ {}^{phantom}_{USimg}T = \left({}^{Polaris}_{phantom}T\right)^{-1} {}^{Polaris}_{USprobe}T \, {}^{USProbe}_{USimg}T \quad (1) $$

Figure 4 shows the system architecture for US images' acquisition. The pixel spacing of each recorded US image is $Epix_x = 0.126872\,mm$ and $Epix_y = 0.119093\,mm$ in the x and y directions, respectively.

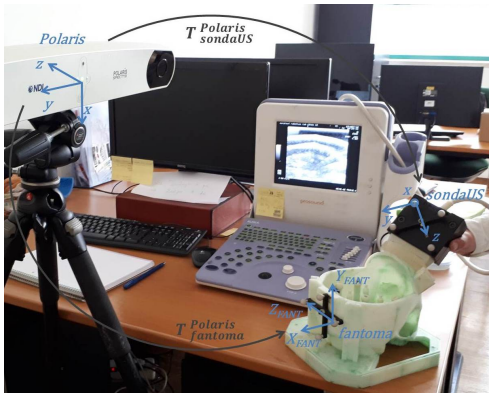

Figure 4: System architecture for US images' acquisition and representation of the transformations between different reference frames: *Polaris* - Polaris base, *US probe* - Polaris' tool marker coupled to the US probe, *phantom* - Polaris' tool marker coupled to the phantom.

4.3.3 CT images' acquisition

The phantom was also CT scanned. The voxel spacing of each recorded CT image is $Evox_x = Evox_y = 0.5469\,mm$ and $Evox_z = 1.25\,mm$ in the x, y and z directions, respectively.

4.3.4 Target's localisation

It is also important to identify the phantom targets' centre localisation as they are needed to compute TRE and evaluate the registration algorithm accuracy. Their poses can be determined with a pointer tracked by Polaris.

5. Segmentation Algorithms

Segmentation is a crucial step before registration and consists of the point set extraction that identifies the outer border of the phantom's skull in both CT and US images. Then, a relation between the two point sets, that actually represent the same surface, can be estimated during the registration step.

5.1. CT images

- 3D reconstruction

The first step is to build a 3D reconstruction of the phantom from the obtained DICOM file.

- Division in 4 subvolumes

The reconstruction is divided in 4 subvolumes to simplify the following steps. These subvolumes include the phantom's right and left side zones, frontal area and interior zone with the targets.

- Scan along rows and columns

In order to identify the transition from the background - black - to the outer border of the phantom's skull - white - within CT images, a scan along rows and columns is performed in different directions according to the considered subvolume, since all scans go from the phantom's outside through the inside. In each scan the intensity difference between two consecutive voxels is computed and the highest value corresponds to the desired border location.

- Outliers' removal

This step was performed manual and occasionally.

- Final result

A demonstration of some CT segmentation algorithm steps is shown in Figure 5, where (a) the considered subvolume - in blue - includes (b) the 3D reconstruction of the phantom's right side that is going to be scanned (c) along horizontal rows from outside to inside to segment (d) the outer right side border of the phantom.

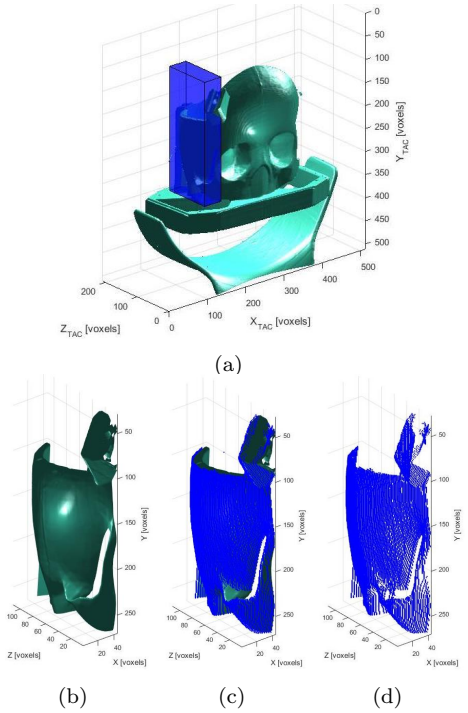

(a)

(b) (c) (d)

Figure 5: Application of the CT segmentation algorithm scan step to the 3D reconstruction of the phantom's right side.

Figure 6 shows the final result after applying the CT segmentation algorithm to the DICOM information contained inside the considered 4 subvolumes.

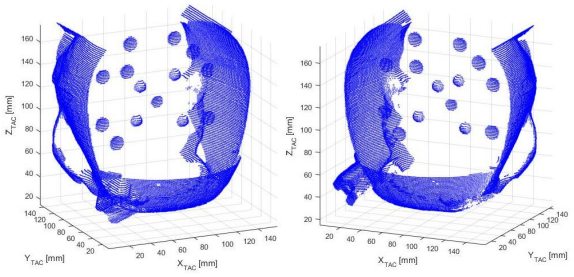

Figure 6: Application of the CT segmentation algorithm to the phantom's CT DICOM file.

5.2. US images

- Crop

The images obtained through the frame grabber represent the entire US machine screen. One must crop the regions that don't provide useful information and keep the pixels that describe the border that must be segmented.

- Filtration

Since US images are characterised with high levels of noise, it is necessary to smooth them so that the border detection algorithm is not sensitive to small intensity differences that don't define the structure one wants to identify. A Gaussian filter is applied to the cropped image, blurring it by replacing each pixel intensity by the mean intensity of the neighbour' pixels.

- Contrast

Then, contrast is applied to enhance the transition from black (gel) to white (outer border of the phantom's skull), by saturating both superior and inferior colour limits. This way, black regions become darker and white regions become brighter.

- Scan along columns

An up-down scan through each image column may now take place, selecting the pixel's position that corresponds to the highest intensity difference value between two consecutive pixels. If more than one value above a pre-determined threshold is found, only the uppest one is considered.

- Outliers' removal

If some outliers occur, a fifth step has to be performed. This step includes the clustering algorithm DBSCAN (Density-Based Spatial Clustering of Applications with Noise) [22] that groups point sets according to their density in space. This algorithm requires only 2 parameters - the radius to be considered around each point and the minimum number of points that defines a cluster.

- Final result

A demonstration of some US segmentation algorithm steps is shown in Figure 7, where (a) a set of 200 cropped images spatially displayed is subjected to filtering, contrast and column scanning, followed by (b) the identification - in orange - of the outer border of the phantom's skull where (c) the resulting points are subjected to DBSCAN algorithm giving rise to (d) the final result.

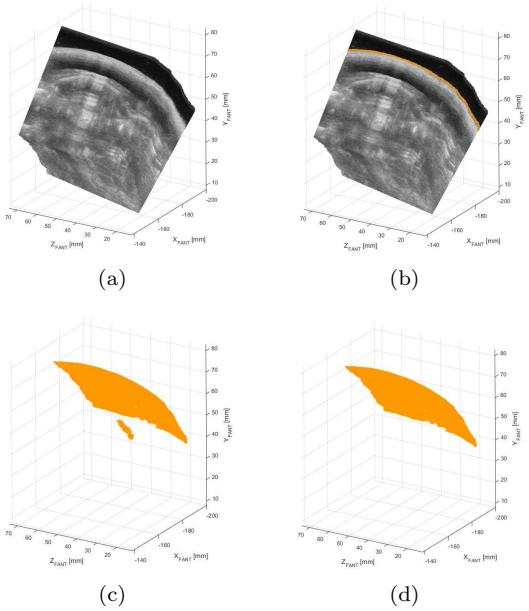

Figure 7: Application of some US segmentation algorithm steps to an example set of acquired and already cropped US images.

Figure 8 shows the final result after applying the US segmentation algorithm to all sets of acquired phantom's US images and its measured targets' position, mentioned in 4.3.4.

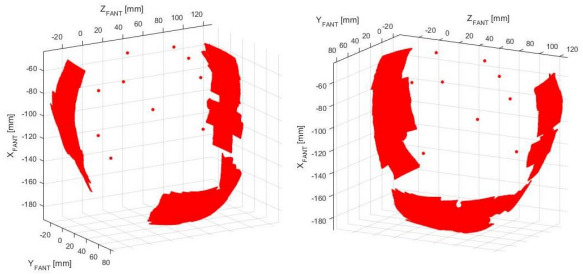

Figure 8: Application of the US segmentation algorithm to the phantom's acquired US images and its targets' localisation, measured separately.

Section 6 describes two ways to register both point clouds represented in Figures 6 and 8.

6. ICP Registration Algorithm

Registration is the process that determines a geometrical transformation $T = \left(\vec{R}, \vec{t}\right)$ that rigidly rotates - $\vec{R}$ is the rotation matrix - and translates - $\vec{t}$ is the translation vector - the corresponding points from one space to the other, resulting in the accurate alignment between corresponding points so that attributes associated with those points can be viewed and analysed jointly. During this process, one point cloud is considered fixed - F - while the other is movable - M - in order that the latest can be registered to the fixed one: $F = T(M)$ e $M = T^{-1}(F)$.

The most accurate way to find T and register two scattered point clouds remains a research hotspot of many researchers at present [23]. Although, the most unanimously accepted, used and exploited algorithm by the scientific community has been the Iterative Closest Point (ICP) algorithm, proposed in 1992 by Besl e McKay [24].

ICP is not only an iterative algorithm as the $\vec{R}$ and $\vec{t}$ parameters are updated in each iteration, but also recursive since it needs the values of those previous parameters to calculate the present ones. Two variants of the ICP will be explored in this work - Point to Point and Point to Plane.

6.1. Point to Point

Point to Point ICP variant only requires the spatial localisation of all points and the computation of distances among them. It computes the transformation matrix that minimises the mean squared distance among the point clouds' closest point pairs.

The repeated steps for each iteration k are:

- Find the closest points

For each point $\vec{m} \in M_k$, one must find the closest point $\vec{f} \in F$. In other words, for each point $\vec{m} \in M_k$ the distance d to each point of F is calculated and the closest one is selected this way:

$$d\left(\vec{m}, F\right) = \min_{f \in F} \left\| \vec{f} - \vec{m} \right\| \tag{2}$$

where d is the Euclidean distance. If $\vec{p} \in F$ is the closest point to $\vec{m} \in M_k$ so that $d\left(\vec{m}, \vec{p}\right) = d\left(\vec{m}, F\right)$, then $P_k = \{\vec{p}_1, \vec{p}_2, \ldots, \vec{p}_{N_M}\}$ includes all $\vec{f} \in F$ points that are the closest of each $\vec{m} \in M_k$. If D is considered a "minimum distance operator", then, for each iteration k:

$$P_k = D\left(M_k, F\right) \tag{3}$$

- Compute the transformation matrix

Estimated the closest point pairs $(\vec{m}, \vec{p})$, one must compute the "best" transformation matrix T_k that registers M_0 in F. By "best" one means the transformation matrix that minimises the mean squared

distance between $T_k(M_0)$ and F, whose rotation matrix $\vec{R}_k$ and translation vector $\vec{t}_k$ are calculated this way:

$$\left(\vec{R}_k,\, \vec{t}_k\right) = \min \sum_{i=1}^{N_M} \|T_k \vec{m}_i - \vec{p}_i v\|^2 =$$

$$= \min \sum_{i=1}^{N_M} \left\| \vec{R}_k \vec{m}_i + \vec{t}_k - \vec{p}_i \right\|^2 \quad (4)$$

This optimisation problem is solved using the Least Square Method. If R is considered an "optimal registration operator", then, for each iteration k:

$$(T_k, rmse_k) = R\,(M_0, P_k) \quad (5)$$

where T_k is the transformation matrix of iteration k, $rmse_k$ is the root mean square error of the registered point clouds in iteration k, M_0 is the original movable point cloud and P_k is the F closest point set of M points.

- Apply the transformation matrix

The localisation of each point $\vec{m} \in M_0$ from the original movable point cloud is updated:

$$M_{k+1} = T_k(M_0) \quad (6)$$

- Verify the termination criteria

This process keeps going until at least one of the two termination criteria is reached: maximum number of iterations and/or rotation and translation tolerances, all previously defined. The algorithm stops when the maximum number of iterations is reached and when the average difference between estimated rigid transformations in the three most recent consecutive iterations falls below the specified tolerance value.

6.2. Point to Plane

Point to Plane ICP variant was proposed in 1992 by Chen and Medioni [25] and requires not only the spatial localisation of all points and the distances' computation among them, but also the extraction of each point normal vector. It computes the transformation matrix that minimises the mean squared distance between points from one point cloud and the projection of those points through their normal vectors' direction on a local approximate plane of the other point cloud.

The main improvement with respect to the original ICP is that it does not require direct correspondence among points from both point clouds, since the transformation matrix is not calculated point to point, but point to plane.

The repeated steps for each iteration k are:

- Calculate the normal vectors

Normal vectors $\vec{n}_m$ and $\vec{n}_f$ of each point of point clouds M e F, respectively, are calculated.

- Find the points' correspondence

For each point $\vec{m} \in M_k$, one must find the correspondence point SF. In other words, find the intersection of the line $\vec{r}_m$ that passes in $\vec{m} \in M_k$ through its normal vector direction $\vec{n}_m$ and the SF surface so that the intersection point $\vec{f}\,' \in SF$ is:

$$\vec{f}\,' = \left(T^{k-1}\vec{r}_m\right) \cap SF \quad (7)$$

- Estimate a tangent plane

The next step is to estimate a tangent plane at the intersection point $\vec{f}\,' \in SF$ so that:

$$S_{f\,'} = \{\vec{n}_f\,(f\,' - s) = 0\} \quad (8)$$

- Compute the transformation matrix

For each estimated tangent plane, the algorithm finds the transformation matrix T_k that best registers point clouds M_0 e F, according to the following optimisation problem:

$$T_k = \min \sum_{i=1}^{N_M} d^2\,(T_k\,\vec{m}_i, S_{f\,'}) \quad (9)$$

where d is the Euclidean distance between each point $\vec{m} \in M_k$ and the tangent plane. This is also solved using the Least Square Method.

- Apply the transformation matrix

The localisation of each point $\vec{m} \in M_0$ from the original movable point cloud is updated:

$$M_{k+1} = T_k(M_0) \quad (10)$$

- Verify the termination criteria

The termination criteria is the same as for the original ICP algorithm, and has already been presented above.

7. Results and Discussion

7.1. Application of the Segmentation Algorithms

The final results of the application of the segmentation algorithms to the acquired phantom's CT and US images are shown in Figures 6 and 8, respectively.

7.2. Application of the Registration Algorithms

In the following Figures 9, 10, 11 and 12, the blue point cloud is the resulting CT segmented point cloud. The green point cloud is a subset of the blue one and is the one considered to be movable. The red point cloud is the resulting US segmented point cloud and is the one considered to be fixed. The blue targets are included in the resulting CT segmented point cloud. The green targets were manually selected from the resulting CT segmented point cloud. The red targets were collected with Polaris.

TRE is the distance between the red and green targets, after registration. Every movable point cloud started from the same initial approximation.

7.2.1 "Ideal" registration matrix

In order to estimate the best alignment between the localisation of the targets' centre in the phantom (Figure 8) and CT (Figure 6) reference frames, both target clouds were registered. Since the targets have direct correspondence, the point to point ICP algorithm was used. The resulting transformation matrix T_{total} is expressed in Equation 11 and the final alignment is represented in Figure 9.

$$T_{total} = T_{CT}^{phantom} = \\ = \begin{bmatrix} 0.0081 & 0.0499 & 0.9987 & -218.7512 \\ 0.0419 & -0.9979 & 0.0495 & 79.5797 \\ 0.9991 & 0.0415 & -0.0102 & -35.4463 \\ 0.0000 & 0.0000 & 0.0000 & 1.0000 \end{bmatrix} mm \quad (11)$$

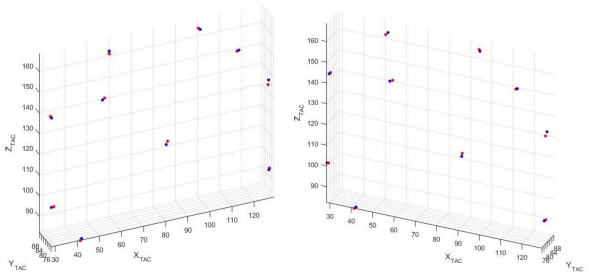

(a) (b)

Figure 9: Point to point ICP registration of the phantom targets after 4 iterations, in the phantom's reference frame. $RE = TRE = 1.3069\,mm$.

This result means that using T_{total} to achieve the best possible alignment of the phantom targets the resulting error is $RE = TRE = 1.3069\,mm$, so any future alignment between the segmented point clouds will include a basis error of 1.3 mm. The result of the application of the "ideal" transformation matrix T_{total} to the point clouds represented in Figures 8 and 6 is shown in Figure 10.

As can be seen, in the best alignment the red and green point clouds do not touch each other as they were supposed to, since they both represent the same surface. This fact is due to the error propagation from the pivoting and probe-image calibration results to the temporal synchronisation of all devices, passing through the manual calculation of pixel spacing in US images.

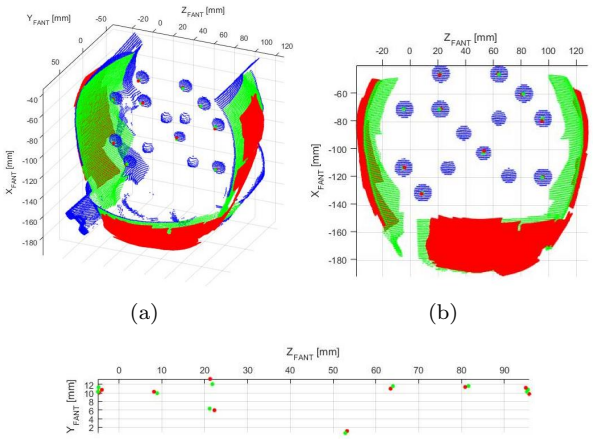

(a) (b)

(c)

Figure 10: Result of the application of T_{total} to the resulting CT and US segmented point clouds. $TRE = 1.3069\,mm$.

7.2.2 Point to Point ICP

The result of the point to point ICP registration algorithm to the point clouds represented in Figures 8 and 6 is shown in Figure 11.

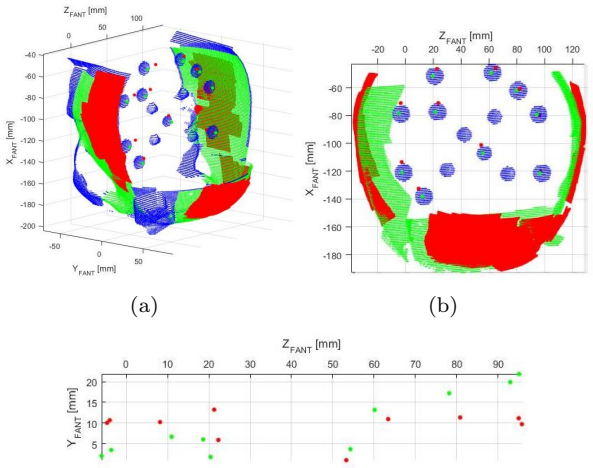

(a) (b)

(c)

Figure 11: Point to point ICP registration of the resulting CT and US segmented point clouds, after 583 iterations. $RE = 2.9275\,mm$ and $TRE = 8.4987\,mm$.

7.2.3 Point to Plane ICP

The result of the point to plane ICP registration algorithm to the point clouds represented in Figures 8 and 6 is shown in Figure 12.

8. Conclusions

The present work suggests a new registration technique that surpasses obstacles presented by current

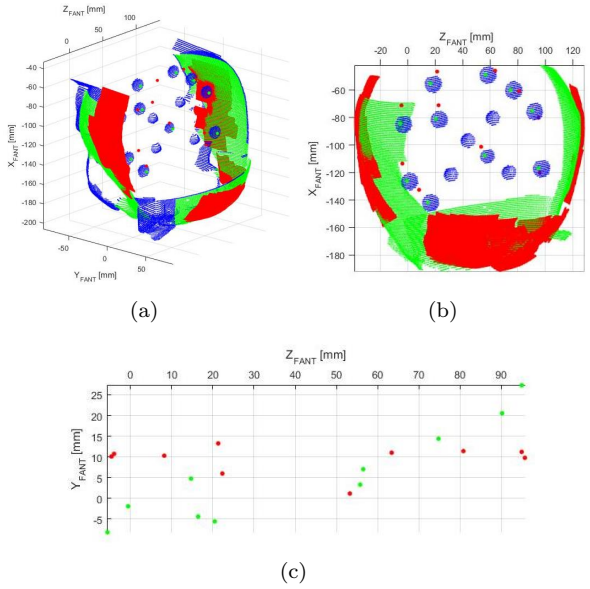

Figure 12: Point to plane ICP registration of the resulting CT and US segmented point clouds, after 1000 iterations. $RE = 4.5136\,mm$ e $TRE = 14.0845\,mm$.

registration techniques, using preoperative CT images with intraoperative ultrasound ones. US scans acquire a large number of points, can directly identify the outer skull surface without skin limitations, are non-invasive, require no radiation and are easily incorporated in a surgical environment.

These findings show successfully created segmentation algorithms for acquired CT and US images. The registration results show that in the best possible alignment, both segmented point clouds do not touch each other. This is due to the error propagation from the pivoting and probe-image calibration results to the temporal synchronisation of all devices, passing through the manual calculation of pixel spacing in US images.

However, in sum, the final outcome of this work constitutes a good foundation for further development and enhancement of a new image-to-patient registration method and may motivate the elimination of any invasive one in neuronavigation assisted surgeries.

9. Future Work

Suggestions and recommendations for the continuity of this project, so as to improve the proposed image-to-patient registration technique, include:

- Use updated phantom CT images, including its targets, to directly identify their centres' localisation.
- Use a probe-image calibration technique with no included manual steps to be less susceptible to human subjectivity and errors.
- Include a scaling factor on the estimated final transformation matrix, besides rotation and translation.
- Include surface features, as curvatures, in the registration algorithm to surpass the fact that the skull is practically spherical and does not present geometrical characteristics sufficiently specific to allow the accurate alignment between surfaces.
- Apply the "recognition of the face contour" surface-based registration method and compare the results with the ones presented here, according to *RE* and *TRE* errors.

References

[1] Alireza Khoshnevisan and Narges Sistany Allahabadi. Neuronavigation: principles, clinical applications and potential pitfalls. *Iranian journal of psychiatry*, 7(2):97, 2012.

[2] Geirmund Unsgaard, Steinar Ommedal, Tomm Muller, Aage Gronningsaeter, and Toril A Nagelhus Hernes. Neuronavigation by intraoperative three-dimensional ultrasound: initial experience during brain tumor resection. *Neurosurgery*, 50(4):804–812, 2002.

[3] René Krishnan, Elvis Hermann, Robert Wolff, Michael Zimmermann, Volker Seifert, and Andreas Raabe. Automated fiducial marker detection for patient registration in image-guided neurosurgery. *Computer Aided Surgery*, 8(1):17–23, 2003.

[4] David W Roberts, John W Strohbehn, John F Hatch, William Murray, and Hans Kettenberger. A frameless stereotaxic integration of computerized tomographic imaging and the operating microscope. *Journal of neurosurgery*, 65(4):545–549, 1986.

[5] G Eggers, J Mühling, and R Marmulla. Image-to-patient registration techniques in head surgery. *International journal of oral and maxillofacial surgery*, 35(12):1081–1095, 2006.

[6] Daniel A Orringer, Alexandra Golby, and Ferenc Jolesz. Neuronavigation in the surgical management of brain tumors: current and future trends. *Expert review of medical devices*, 9(5):491–500, 2012.

[7] U Spetzger, G Laborde, and JM Gilsbach. Frameless neuronavigation in modern neurosurgery. *min-Minimally Invasive Neurosurgery*, 38(04):163–166, 1995.

[8] Hospital da Luz. http://www.hospitaldaluz.pt/lisboa/pt/apoio-a-clientes/saiba-mais-sobre-a-sua-saude/area-de-pesquisa/?contentId=58341. Visited in May 2018.

[9] Heinz-Theo Luebbers, Peter Messmer, Joachim Anton Obwegeser, Roger Arthur Zwahlen, Ron Kikinis, Klaus Wilhelm Graetz, and Felix Matthews. Comparison of different registration methods for surgical navigation in cranio-maxillofacial surgery. *Journal of Cranio-Maxillofacial Surgery*, 36(2):109–116, 2008.

[10] Manning Wang and Zhijian Song. Guidelines for the placement of fiducial points in image-guided neurosurgery. *The International Journal of Medical Robotics and Computer Assisted Surgery*, 6(2):142–149, 2010.

[11] Marcel Ivanov and Alexandru Vlad Ciurea. Neuronavigation. Principles. Surgical technique. *Journal of medicine and life*, 2(1):29, 2009.

[12] Peter WA Willems, Jan W Berkelbach van der Sprenkel, and Cees AF Tulleken. Comparison of adhesive markers, anatomical landmarks, and surface matching in patient-to-image registration for frameless stereotaxy. In *EOS/SPIE European Biomedical Optics Week*, pages 156–163. International Society for Optics and Photonics, 2001.

[13] Kathryn L Holloway, Steven E Gaede, Philip A Starr, Joshua M Rosenow, Viswanathan Ramakrishnan, and Jaimie M Henderson. Frameless stereotaxy using bone fiducial markers for deep brain stimulation. *Journal of neurosurgery*, 103(3):404–413, 2005.

[14] Christian Kremser, Clemens Plangger, Robert Bösecke, Anton Pallua, Franz Aichner, and Stephan R Felber. Image registration of MR and CT images using a frameless fiducial marker system. *Magnetic resonance imaging*, 15(5):579–585, 1997.

[15] DG Thomas and ND Kitchen. Minimally invasive surgery. neurosurgery. *BMJ: British Medical Journal*, 308(6921):126, 1994.

[16] PWA Willems, JW Berkelbach van der Sprenkel, CAF Tulleken, MA Viergever, and MJB Taphoorn. Neuronavigation and surgery of intracerebral tumours. *Journal of neurology*, 253(9):1123–1136, 2006.

[17] Aize Cao, RC Thompson, P& al Dumpuri, BM Dawant, RL Galloway, S Ding, and MI Miga. Laser range scanning for image-guided neurosurgery: Investigation of image-to-physical space registrations. *Medical physics*, 35(4):1593–1605, 2008.

[18] J Michael Fitzpatrick, Jay B West, and Calvin R Maurer. Predicting error in rigid-body point-based registration. *IEEE transactions on medical imaging*, 17(5):694–702, 1998.

[19] Manning Wang and Zhijian Song. Improving target registration accuracy in image-guided neurosurgery by optimizing the distribution of fiducial points. *The International Journal of Medical Robotics and Computer Assisted Surgery*, 5(1):26–31, 2009.

[20] Zhe Li, Jian-Guo Zhang, Yan Ye, and Xiaoping Li. Review on factors affecting targeting accuracy of deep brain stimulation electrode implantation between 2001 and 2015. *Stereotactic and functional neurosurgery*, 94(6):351–362, 2016.

[21] Diane M Muratore and Robert L Galloway. Beam calibration without a phantom for creating a 3-D freehand ultrasound system. *Ultrasound in Medicine and Biology*, 27(11):1557–1566, 2001.

[22] Derya Birant and Alp Kut. ST-DBSCAN: An algorithm for clustering spatial-temporal data. *Data & Knowledge Engineering*, 60(1):208–221, 2007.

[23] Ying He, Bin Liang, Jun Yang, Shunzhi Li, and Jin He. An iterative closest points algorithm for registration of 3D laser scanner point clouds with geometric features. *Sensors*, 17(8):1862, 2017.

[24] Paul J Besl and Neil D McKay. Method for registration of 3-D shapes. In *Sensor Fusion IV: Control Paradigms and Data Structures*, volume 1611, pages 586–607. International Society for Optics and Photonics, 1992.

[25] Yang Chen and Gérard Medioni. Object modelling by registration of multiple range images. *Image and vision computing*, 10(3):145–155, 1992.